Digital Signal Processing 21 (2011) 100–109

Contents lists available at ScienceDirect

Digital Signal Processing

www.elsevier.com/locate/dsp

3-D medical image compression using 3-D wavelet coders

N. Sriraam [a,*], R. Shyamsunder [b]

[a] Center for Biomedical Informatics and Signal Processing, Department of Biomedical Engineering, SSN College of Engineering, Chennai, India
[b] Dept. of Electrical and Computing Engineering, National University of Singapore, Singapore

ARTICLE INFO

Article history:
Available online 30 June 2010

Keywords:
Medical image compression
3-D SPIHT
3-D SPECK and 3-D BISK
Symmetric wavelet transform
Decoupled wavelet transform

ABSTRACT

This paper presents compression of 3-D medical images using 3-D wavelet encoders. Four wavelet transforms, namely, Daubechies 4, Daubechies 6, Cohen–Daubechies–Feauveau 9/7 and Cohen–Daubechies–Feauveau 5/3 are used in the first stage with encoders such as 3-D SPIHT, 3-D SPECK and 3-D BISK used in the second stage for the compression and the optimal wavelet–encoder combination is identified. Two versions of wavelet transform, symmetric and decoupled wavelet transform are considered. Experiments are performed using medical test images such as magnetic resonance images (MRI) and X-ray angiograms (XA). The performances of the proposed scheme are evaluated in terms of peak signal-to-noise ratio and bit rate. Further mean structural similarity (MSSIM) index is introduced to evaluate the structural similarity between the original and the reconstructed images. It is found from the test results that the 3-D Cohen–Daubechies–Feauveau 9/7 symmetric wavelet along with the 3-D SPIHT encoder yields the best compression result.

1. Introduction

For teleradiological applications, quality of reconstructed medical images plays a crucial role in diagnosis as well as treatment of patients. In the recent years, the stringent demand of storage and transmission of multidimensional medical images has provoked significant research interest in the filed of medical image compression [1–7]. Compression can be lossless if it provides the exact replica of the original and lossy when incorporates certain quantization [1–7]. For medical image compression, lossy compression is allowed as long as the required diagnostic quality is preserved in the reconstructed images [4–6]. It is known that medical experts prefers 3-D images for analysis as it provides the flexibility of viewing the anatomical cross sections required for accurate detection of abnormalities [1–4]. Several works on 3-D medical image compression have been reported in the literature [1–14]. In [1] Schelkens et al. proposed new compression methods exploiting the quadtree and block-based coding concepts, layered zero-coding principles, and context-based arithmetic coding and have compared the performances of these coders with those of the JPEG2000, 3-D Set Partitioning In Hierarchical Trees (3-D SPIHT) and 3-D Set Partitioned Embedded bloCK (3-D SPECK). They have shown that in the case of lossless compression, the proposed coders give excellent results whereas for lossy compression it provides comparable results. Xiong et al. have studied the lossy and lossless compression of CT and MR volumetric data sets using 3-D integer wavelet transforms. They have modified the 3-D SPIHT and the 3-D Embedded Block Coding with Optimized Truncation (3-D EBCOT) coding schemes and applied them for compressing the medical data and have shown that their method gives comparable results for both lossy and lossless compression [6]. Chao et al. proposed an optimal 3-D coefficient tree structure for 3-D zero tree wavelet video coding and have shown that the 3-D zero tree coding need not be applied symmetrically along all the directions and that the asymmetrical trees can produce higher compression ratio than the symmetrical ones [11]. Gibson et al. have suggested

* Corresponding author. Fax: +91 44 27475063.
E-mail address: sriraamn@ssn.edu.in (N. Sriraam).

1051-2004/$ – see front matter
doi:10.1016/j.dsp.2010.06.002

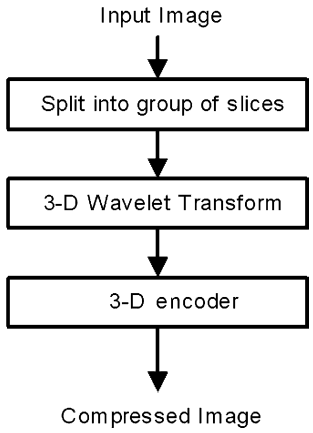

Fig. 1. Block diagram of the 3-D wavelet transform based storage/transmission.

a novel method for compression of angiogram video sequences which is based on the idea that diagnostically significant areas of the image should be allocated the greatest proportion of the total available bit budget. They have incorporated the region of interest (ROI) detection stage and texture modelling stage into the 3-D wavelet and SPIHT framework [12].

3-D SPECK and 3-D binary set splitting with *k*-D trees (3-D BISK) have been used mostly for compression of hyper spectral images. Tang et al. have used 3-D SPECK compression of hyper spectral images, which are sequences of images generated by collecting contiguously spaced spectral bands of data. They have shown that 3-D SPECK gives comparable performance to that of the 3-D SPIHT coder [13]. Fowler and Rucker have given an overview on the major concepts in 3-D embedded wavelet-based compression for hyperspectral imagery including 2-D and 3-D SPECK [14]. They have shown that the performances of the different techniques are roughly similar in terms of rate distortion performance. Lu and Pearlman have used the OB-SPECK algorithm (object based set partitioned embedded block coder) for wavelet coding of arbitrary shaped video objects [15]. The proposed scheme achieves high coding efficiency and preserves the features of an embedded bit stream, low computational complexity and exact bit rate control. Rucker and Fowler have used 3-D BISK for shape adaptive coding of ocean-temperature data. The performance of 3-D BISK is compared to prominent shape-adaptive coders and superior performance is demonstrated [16]. Although several work have been reported for 3-D medical image compression using wavelets, to the extent of author's knowledge, optimal wavelet coders suitable for medical image compression problems has not been explored.

This paper discusses the performance evaluation of 3-D lossy medical image compression using 3-D wavelet transforms followed by 3-D wavelet encoders. Four wavelet transforms, namely, Daubechies 4 (D4), Daubechies 6 (D6), Cohen–Daubechies–Feauveau 9/7 (CDF 9/7) and Cohen–Daubechies–Feauveau 5/3 (CDF 5/3) are used in the first stage with encoders such as 3-D SPIHT, 3-D SPECK and 3-D BISK used in the second stage for the compression. Experiments are performed using magnetic resonance images (MRI) and X-ray angiograms (XA) test images. The performances of the 3-D medical images are evaluated in terms of peak signal-to-noise ratio (PSNR) and bit rate and the optimal wavelet transform–encoder is identified. Fig. 1 shows the block diagram for the compression technique using the 3-D wavelet encoders. First the 3-D medical image is split into groups of slices (GOS). Then the 3-D wavelet transform is applied, followed by 3-D encoding.

2. 3-D wavelet transform

It is known that 3-D wavelet transform can be obtained by applying 1-D wavelet transform along each dimension [11]. If W_x, W_y, W_z represent the wavelet transformations applied along the x, y and z axes then transform of this image is defined as $W = (W_xW_yW_z)_1(W_xW_yW_z)_2 \ldots (W_xW_yW_z)_L$ where L is the number of levels. This is called the 3-D symmetrical wavelet transformation, where all the dimensions are decomposed to equal number of levels by applying wavelet transform alternately to each axis (see Fig. 2) [11]. On the other hand, 3-D wavelet transform can be also be obtained by applying 2-D spatial transform first, followed by wavelet transform on the z axis separately. This can be defined as $W = (W_xW_y)_1(W_xW_y)_2 \ldots (W_xW_y)_L(W_z)_1(W_z)_2 \ldots (W_z)_l$. The spatial axis are decomposed to equal number of levels 'L' but the z axis can be decomposed to 'l' levels which need not be equal to 'L'. This is called the decoupled 3-D wavelet transform or the 3-D wavelet packet transform [11]. For further details one can refer [22]. The lifting approach used for implementing wavelets has been proposed by Sweldens [17]. The major advantage of lifting is the fact that it requires lesser memory and is faster than the general wavelet transform, hence providing a platform for real time applications. 3-D DWT can be realized by applying 1-D DWT along each dimension.

For 1-D wavelet lifting, the input signal is split into and odd and even samples followed by a series of predict (P) and update (U) lifting steps to obtain the low pass (LP) and high pass (HP) coefficients respectively. The LP coefficients represent the coarse values and the HP coefficients represent the detail values in the data [18]. The predict and update

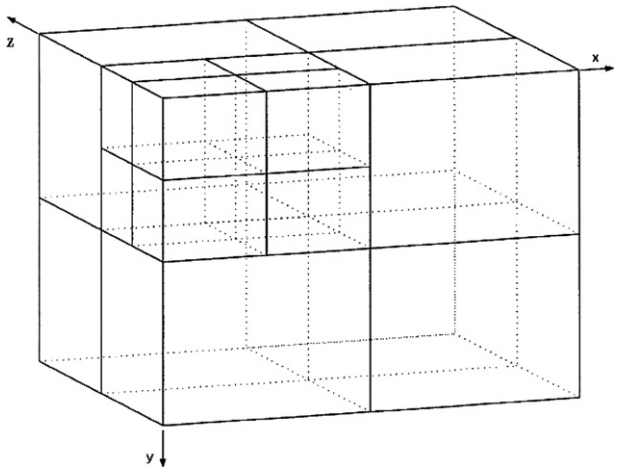

Fig. 2. 3-D symmetric DWT with two levels of decomposition.

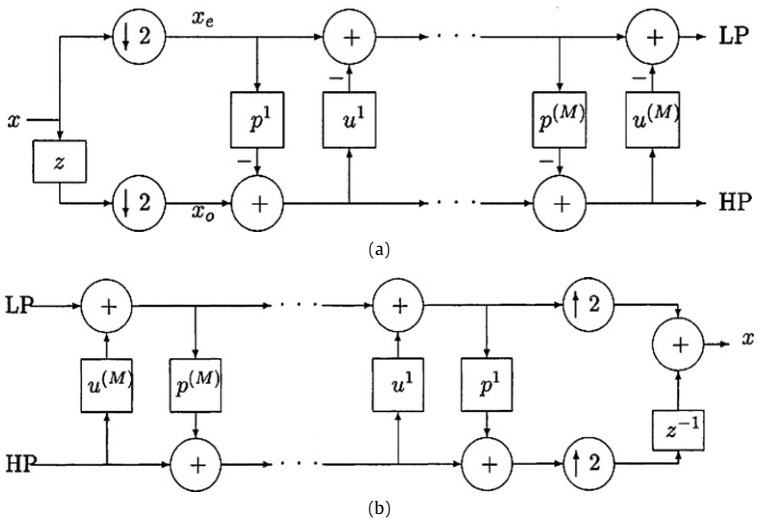

Fig. 3. Wavelet transform: (a) Forward lifting step, (b) inverse lifting step.

steps are sometimes referred to as dual and primal lifting steps. The inverse transform is formed by reversing the steps of the forward transform and flipping the signs. The forward and inverse lifting steps are shown in Fig. 3 [19].

In the predict step, the odd elements are predicted using the even elements. Then the detail coefficient is given by the difference between the original odd value and its predicted value. The detail coefficient replaces the original odd value for further calculations. This can be explained as follows:

If '*d*' represents the detail coefficient and '*s*' represents the coarse coefficient then, the prediction step can be defined as $d_{n-1} = d_n - P(s_n)$, where P is the prediction operator. Similar to the predict step, the update step can be defined as $s_{n-1} = s_n + U(d_{n-1})$, where U is the update operator. The predict and update steps required for the wavelets considered in this paper are given in Table 1 [19,20].

3. Experimental setup and performance evaluation

In medical imaging, 3-D images refer to the time sequence of radiographic images or tomographic slice images of a dynamic object or a volume of tomographic slice image of a static object [23]. In this paper, 3-D data sets refer to the latter case. In other words, the 3-D image can be visualized as 2-D image slices stacked one after the other where each slice shows the progressive variation of a static object. Thus the 3-D medical image is a 3-D rectangular array of voxels, with a value assigned to each voxel [23]. The 3-D medical image data considered in this work are MR and XA images. Samples of XA and MR images with all the 16 slices are shown in Fig. 4.

The slices in each GOS are chosen as 4, 8 and 16. The numbers of decompositions for the symmetric and the decoupled wavelet transform are given in Table 2. The details of the experimental test data used in the performance evaluation of the 3-D wavelets transform are given in Table 3.

Table 1
Forward transforms for lifting based wavelet transforms.

D4	$d_1[n] = d_0[n] - \sqrt{3}s_0[n]$
	$s_1[n] = s_0[n] + \frac{\sqrt{3}}{4}d_1[n] + \frac{\sqrt{3}-2}{4}d_1[n+1]$
	$d_2[n] = d_1[n] + s_1[n-1]$
	$s_2[n] = s_1[n] + \left(\frac{2}{(\sqrt{3}+1)^2} - \frac{\sqrt{2}}{\sqrt{3}+1}\right)d_2[n]$
	$d_3[n] = d_2[n] + \frac{\sqrt{3}+1}{\sqrt{2}}s_2[n]$
D6	$d_1[n] = d_0[n] - \frac{211}{512}s_0[n]$
	$s_1[n] = s_0[n] + \frac{45}{128}d_1[n] - \frac{50}{32}d_1[n-1]$
	$d_2[n] = d_1[n] - \frac{29}{1024}s_1[n] + \frac{63}{128}s_1[n+1]$
	$s_2[n] = s_1[n] + \frac{25}{64}d_2[n]$
	$d_3[n] = d_2[n] + s_2[n]$
CDF 9/7	$d_1[n] = d_0[n] - \frac{203}{128}s_0[n+1] - s_0[n]$
	$s_1[n] = s_0[n] - \frac{217}{4096}d_1[n] - d_1[n-1]$
	$d_2[n] = d_1[n] + \frac{113}{128}s_1[n+1] + s_1[n]$
	$s_2[n] = s_1[n] + \frac{1817}{4096}d_1[n] + d_1[n-1]$
CDF 5/3	$d[n] = d_0[n] - \frac{1}{2}s_0[n+1] + s_0[n]$
	$s[n] = s_0[n] + \frac{1}{4}d[n] + d[n-1]$

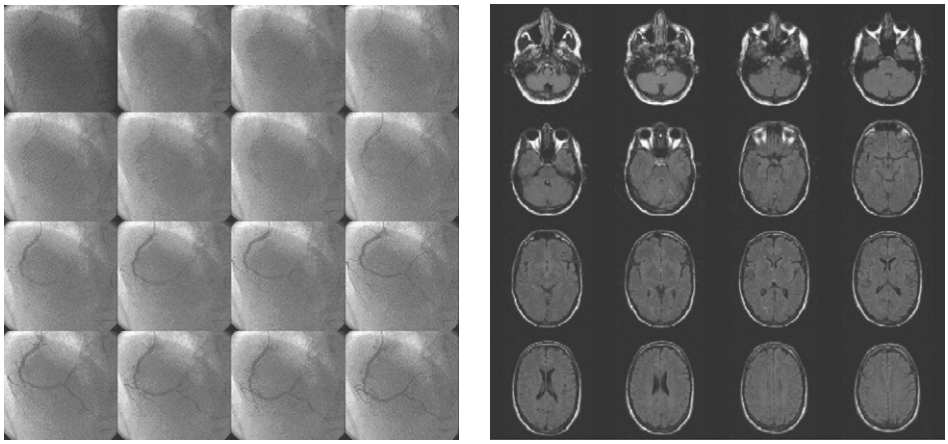

(a) (b)

Fig. 4. (a) Sample of XA image, (b) sample of MR brain image.

Table 2
Number of decomposition levels.

Wavelet transform	GOS size	No. of spatial decompositions		No. of temporal decompositions (for both MR and XA)
		MR (spatial size 256×256)	XA (spatial size 512×512)	
Symmetric	4	1	1	1
	8	2	2	2
	16	3	3	3
Decoupled	4	7	8	1
	8	7	8	2
	16	7	8	3

Table 3
Test data used for the experiments.

Modality	Resolution (2-D)	Total number of slices	No. of patient data sets
MR image	256×256	16	10
XA image	512×512	16	10

Table 4
Compression results for GOS of 16 slices for XA images.

3-D encoder	Bit rate	Symmetric				Decoupled			
		CDF 9/7	CDF 5/3	D4	D6	CDF 9/7	CDF 5/3	D4	D6
SPIHT	0.1	***20.39***	20.42	20.25	20.1	20.24	20.81	20.4	20.2
	0.5	***26.58***	26.22	25.58	25.6	25.85	25.63	24.79	24.65
	1	***32.35***	31.24	30.2	30.25	30.55	28.3	28.4	27.56
	1.5	***39.03***	38.75	38.2	37.59	35.86	34.58	34.21	33.65
	2	***44.9***	42.74	42.12	41.56	42.06	39.65	38.5	38.12
	3	***57.23***	56.8	55.89	54.26	51.43	48.2	47.21	47.11
BISK	0.1	20.55	20.12	17.85	19.52	21.23	20.05	21.1	20.8
	0.5	26.21	25.88	25.26	24.52	23.85	22.2	22.9	22.5
	1	32.2	31.1	30.23	30.12	27.06	26.2	27.1	26.56
	1.5	38.12	37.23	37.11	36.58	27.53	27.44	27.57	27.32
	2	44.55	43.25	42.25	41.65	28.52	28.38	28.5	28.1
	3	55.12	53.12	52.25	52.1	32.21	31.96	32.2	31.2
SPECK	0.1	20.25	20.1	20.21	20.5	20.23	20.05	20.1	20.8
	0.5	26.1	25.56	25.1	25.32	23.85	22.1	22.5	22.3
	1	31.56	30.91	30.1	30.21	26.16	26.12	26.8	26.46
	1.5	36.52	35.23	34.56	34.9	27.43	27.54	27.47	27.34
	2	42.23	42.1	42.22	41.23	28.42	28.56	28.45	28.14
	3	54.56	54.21	54.2	53.69	32.23	31.9	32.23	31.25

Table 5
Compression results for GOS of 8 slices for XA images.

3-D encoder	Bit rate	Symmetric				Decoupled			
		CDF 9/7	CDF 5/3	D4	D6	CDF 9/7	CDF 5/3	D4	D6
SPIHT	0.1	***18.39***	18.32	18.25	18.1	18.24	18.1	18.24	18.28
	0.5	***24.58***	24.42	23.58	23.6	23.75	23.52	22.65	22.54
	1	***30.35***	30.1	28.7	29	28.5	26.37	26.41	25.61
	1.5	***37.03***	36.5	36.2	35.59	33.68	32.81	32.21	31.12
	2	***42.9***	41.4	40.2	40.5	40.16	37.6	36.51	36.23
	3	***55.23***	54.28	53.89	53.26	48.19	46.28	45.16	45.47
BISK	0.1	18.15	18.12	17.5	18.1	18.2	18.09	18.05	17.58
	0.5	24.21	23.88	22.26	22.52	21.5	21.2	21.8	21.35
	1	30.2	30.1	28.2	28.12	24.26	24.2	24.1	24.56
	1.5	36.12	36.23	35.17	35.18	25.23	25.24	25.7	25.2
	2	42.55	42.25	40.51	40.36	27.52	27.38	27.58	27.21
	3	53.12	52.12	51.25	51.21	31.21	30.62	31.2	30.52
SPECK	0.1	18.25	18.21	17.59	18.06	18.11	17.80	17.95	17.28
	0.5	24.17	23.8	22.35	22.65	21.15	21.32	21.6	21.3
	1	29.82	29.17	28.32	28.1	24.16	24.22	24.11	24.35
	1.5	35.72	34.23	34.87	35.42	24.98	25.2	25.32	24.98
	2	41.55	41.25	40.59	40.33	27.1	27.2	27.65	27.62
	3	53.18	52.28	51.35	51.28	31.1	30.3	31.05	31.1

The parameters that are used for the performance comparison are peak signal-to-noise ratio (PSNR) and bit rate (BR) defined as in (1) and (2) respectively [21].

$$\text{PSNR (dB)} = \frac{20 \times \log_{10}(\text{Maximum pixel value})}{\sqrt{\text{MSE}}} \tag{1}$$

MSE in (1) represents the mean squared error of the image defined as

$$\text{MSE} = \frac{1}{N} \times \sum_i \sum_j \big(f(i,j) - F(i,j)\big)^2 \tag{2}$$

where N is the total number of pixels, $F(i,j)$ denotes the pixel value in the reconstructed image and $f(i,j)$ is the pixel value in the original image.

$$\text{BR (bpp)} = \frac{\text{Size of the compressed image in bits}}{\text{Total no of pixels}} \tag{3}$$

Tables 4–9 show the performance of the 3-D XA and MRI images with 16, 8 and 4 slices respectively in terms of PSNR at different bit rates. Different symmetric and decoupled 3-D wavelet transforms are used in the first stage and different 3-D encoders are used in the second stage and the results are reported for all possible combinations.

Table 6
Compression results for GOS of 4 slices for XA images.

3-D encoder	Bit rate	Symmetric				Decoupled			
		CDF 9/7	CDF 5/3	D4	D6	CDF 9/7	CDF 5/3	D4	D6
SPIHT	0.1	***16.39***	15.32	16.25	16.1	15.24	16.1	16.24	16.28
	0.5	***22.58***	22.42	21.58	22.6	21.75	21.52	21.75	20.54
	1	***28.35***	28.1	26.7	29	26.5	25.37	25.34	24.36
	1.5	***34.03***	33.5	31.2	32.59	30.8	30.81	30.52	30.12
	2	***40.9***	39.4	38.2	37.5	37.16	36.56	35.95	35.63
	3	***50.23***	49.28	49.89	48.26	43.19	44.28	43.16	44.74
BISK	0.1	16.9	15.32	16.15	15.51	15.2	15.9	15.51	15.11
	0.5	21.8	22.2	21.5	21.96	20.5	20.42	20.88	20.55
	1	27.35	27.1	26.57	27.9	23.26	22.98	22.58	22.62
	1.5	33.93	33.55	30.98	33.15	24.23	23.4	23.97	23.58
	2	40.59	39.64	38.42	38.15	26.52	25.81	25.58	25.21
	3	49.3	48.2	48.9	48.26	30.21	29.62	29.2	29.52
SPECK	0.1	16.29	15.32	16.25	16.51	15.2	15.9	15.51	15.11
	0.5	21.89	21.8	21.15	21.6	20.5	20.42	20.88	20.55
	1	27.5	26.1	25.57	26.23	23.26	22.98	22.58	22.62
	1.5	33.38	32.59	30.1	31.5	24.23	23.4	23.97	23.58
	2	40.1	38.64	38.2	38.75	26.52	25.81	25.58	25.21
	3	47.98	47.2	46.9	46.26	30.21	29.62	29.2	29.52

Table 7
Compression results for GOS of 16 slices for MR images.

3-D encoder	Bit rate	Symmetric				Decoupled			
		CDF 9/7	CDF 5/3	D4	D6	CDF 9/7	CDF 5/3	D4	D6
SPIHT	0.1	***22.92***	22.42	22.25	22.13	22.24	22.81	22.4	22.22
	0.5	***28.83***	28.22	27.58	27.16	27.85	27.63	26.79	26.11
	1	***34.51***	33.24	32.2	32.25	32.55	29.3	30.4	29.98
	1.5	***42.10***	40.75	40.12	39.59	37.86	35.58	36.21	35.59
	2	***47.19***	46.74	46.12	45.6	44.06	41.65	39.5	39.21
	3	***56.23***	56.18	56.89	56.26	53.43	50.21	47.1	46.91
BISK	0.1	22.2	22.12	21.75	21.11	22.3	22.05	22.1	22.8
	0.5	28.13	27.22	27.88	26.16	24.88	24.29	24.9	24.5
	1	34.41	33.4	33.1	32.5	26.26	26.21	27.1	27.3
	1.5	41.40	41.15	40.2	40.11	28.33	28.44	28.57	28.32
	2	46.49	46.4	45.28	44.6	29.12	29.3	29.45	29.12
	3	55.23	55.18	54.9	54.36	33.24	33.6	33.2	33.22
SPECK	0.1	22.12	21.12	21.75	21.15	21.3	21.05	21.1	21.8
	0.5	27.78	26.22	27.88	26.16	24.68	24.19	24.91	24.65
	1	34.1	34.1	33.41	32.1	26.26	26.21	27.1	27.3
	1.5	42.10	41.1	40.12	40.11	28.35	28.49	28.51	28.52
	2	46.29	46.41	45.8	44.69	29.29	29.37	29.56	29.82
	3	55.3	54.78	53.98	53.67	33.4	33.7	33.12	33.62

It can be seen from Tables 4 to 9 that the symmetric wavelets perform better than their decoupled wavelet counterpart for both XA and MRI test images. Among the four wavelets the CDF 9/7 gives the best result. Among the encoders the 3-D SPIHT gives the best result. It is also observed that the GOS of 16 slices gives the best result.

4. Discussion

A major design of any compression scheme is to obtain the best visual quality with minimum bit utilization. The parameter, peak signal-to-noise ratio is generally used for assessing the quality of the reconstructed image thereby trade off between the quality and the bit rate can be established. Fig. 5 shows the plot indicating the average values of PSNR obtained for MRI and XA images as stated in Tables 4 and 7 for different bit rate. Although [1–14] discuss the 3-D image compression problems, only [1] and [5] address the compression of 3-D medical images. The results obtained using the applied various wavelet based transforms and encoders are compared with the 3-D transforms such as discrete Hartley transform (DHT), discrete cosine transform (DCT) and discrete Fourier transform (DFT) as reported in [26]. Further the fidelity results are also compared with different versions of JPEG standards, JPEG-LS, JPEG 2000, JPEG2K-3D [1,25].

It can be seen from Fig. 5 that the increase in bit rate results in improvement in quality of the reconstructed image. The performance of the wavelet based algorithms yields better results than JPEG and other 3-D transforms. It can be concluded that the user can fix the bit rate depending on his reconstructed image quality requirements.

Table 8
Compression results for GOS of 8 slices for MR images.

3-D encoder	Bit rate	Symmetric				Decoupled			
		CDF 9/7	CDF 5/3	D4	D6	CDF 9/7	CDF 5/3	D4	D6
SPIHT	0.1	***20.8***	20.42	20.25	20.13	20.24	20.48	20.4	20.28
	0.5	***26.8***	26.22	25.8	25.16	25.85	25.63	25.79	25.11
	1	***32.45***	31.21	31.2	31.25	30.55	28.3	28.4	28.98
	1.5	***40.15***	38.7	39.12	39.59	35.86	34.58	34.21	34.59
	2	***45.21***	44.75	44.92	44.6	42.06	40.5	39.15	38.21
	3	***54.25***	54.12	53.89	53.26	51.43	48.2	45.1	45.91
BISK	0.1	20.5	20.2	18.51	19.2	20.23	20.25	20.17	20.8
	0.5	26.2	25.8	25.61	24.12	23.85	22.23	22.91	22.5
	1	32.12	31.21	30.13	30.32	27.06	26.21	27.13	26.56
	1.5	38.72	37.73	37.13	36.38	27.83	27.44	27.57	27.32
	2	44.25	43.95	42.26	41.25	28.52	28.38	28.54	28.1
	3	52.12	52.12	51.25	51.21	32.21	31.96	32.25	31.2
SPECK	0.1	20.51	20.27	18.39	19.2	20.23	20.27	20.1	20.1
	0.5	25.92	25.83	25.62	24.12	25.85	22.91	22.71	22.29
	1	31.92	31.29	30.39	30.28	27.06	26.51	27.13	26.62
	1.5	39.1	37.75	37.13	36.38	27.83	27.94	27.51	27.82
	2	45.1	44.95	44.26	43.25	28.52	28.48	28.12	28.51
	3	53.5	53.12	53.25	51.21	32.21	31.76	31.98	31.2

Table 9
Compression results for GOS of 4 slices for MR images.

3-D encoder	Bit rate	Symmetric				Decoupled			
		CDF 9/7	CDF 5/3	D4	D6	CDF 9/7	CDF 5/3	D4	D6
SPIHT	0.1	***17.97***	17.2	17.5	17.31	17.41	17.14	17.44	17.81
	0.5	***24.8***	24.49	24.18	23.96	23.51	23.22	23.31	23.12
	1	***30.35***	30.13	28.71	29.3	28.15	27.22	27.43	26.63
	1.5	***37.03***	36.15	36.52	35.57	34.26	33.32	33.22	32.44
	2	***42.9***	41.4	40.2	40.5	40.46	37.26	36.15	36.25
	3	***48.23***	47.28	47.1	47.26	45.59	45.22	45.11	45.46
BISK	0.1	17.15	17.12	17.12	17.1	16.2	16.09	16.75	16.56
	0.5	24.21	23.88	22.26	22.52	21.5	21.62	21.28	21.55
	1	30.12	30.1	28.2	28.12	24.26	24.27	24.61	24.52
	1.5	36.19	36.23	35.17	35.18	25.23	25.24	25.7	25.12
	2	42.15	42.25	40.51	40.36	27.52	27.38	27.58	27.11
	3	47.12	47.12	47.25	47.21	30.21	29.62	29.2	29.52
SPECK	0.1	17.25	17.21	16.99	17.06	16.11	16.81	16.5	16.28
	0.5	24.17	23.8	22.35	22.65	21.15	21.32	21.6	21.37
	1	29.82	29.17	28.32	28.1	24.16	24.22	24.11	24.35
	1.5	35.72	34.23	34.87	35.42	24.98	25.24	25.32	24.98
	2	41.55	41.25	40.59	40.33	27.13	27.22	27.65	27.62
	3	47.18	52.28	51.35	51.28	31.14	30.31	31.05	30.99

It is well known that the perceived visual quality of the reconstructed image cannot be justified using MSE. It has been shown by the author [25] that the reconstructed image quality can be very well assessed by the parameter, mean structure similarity index (MSSIM index) [24]. MSSIM index is an image quality assessment parameter based very much on the characteristics of HVS and measures the structural similarity rather than error visibility between two images. The SSIM is defined as

$$\mathrm{SSIM}(i,i') = \frac{(2\mu_i\mu_{i'} + C_1) + 2\sigma_{ii'} + C_2}{(\mu_i^2\mu_{i'}^2 + C_1)(\sigma_i^2\sigma_{i'}^2 + C_2)} \tag{4}$$

where i and i' are spatial patches (windows) of original image I and reconstructed image I' respectively, μ_i and $\mu_{i'}$ are the mean intensity values of i and i' respectively, σ_i and $\sigma_{i'}$ are standard deviation of i and i' respectively, and C_1, C_2 are constants. The mean value is given by

$$\mathrm{MSSIM}(I,I') = \frac{1}{M}\sum_{j=1}^{M}\mathrm{SSIM}\left(i_j i'_j\right) \tag{5}$$

where M is the number of windows of the image. Fig. 6 shows the plot of bit rate vs MSSIM index for different compression schemes.

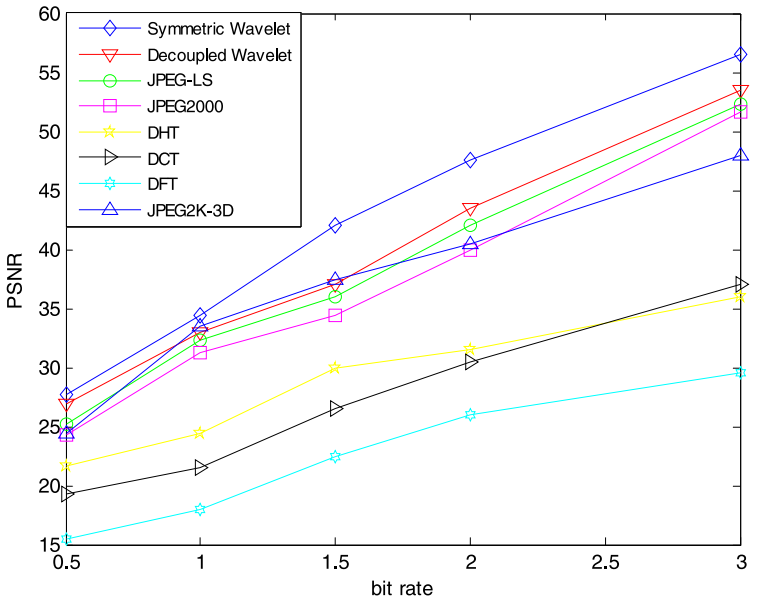

Fig. 5. Rate distortion plot.

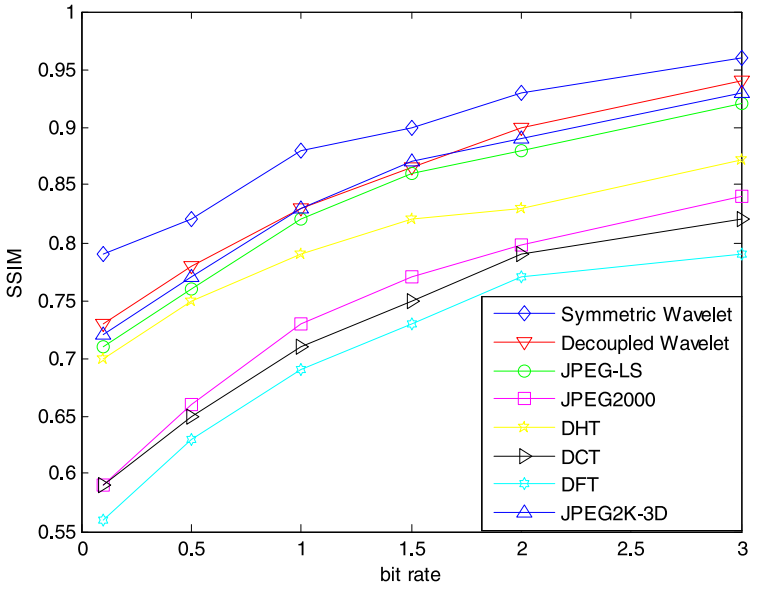

Fig. 6. Plot of bit rate vs MSSIM index.

From the plot shown in Fig. 6, symmetric wavelet outperforms other methods. It can be further seen that for high bit rates the value of MSSIM index reaches closely to one.

In order to determine the efficiency of the wavelet technique, processing time (PT in seconds) which is based on encoding and decoding time period of the wavelet algorithm is calculated for different GOF. A new parameter, called computational efficiency (CE) as defined in (6) is used to evaluate the overall performance.

$$\mathrm{CE} = \frac{\mathrm{PSNR}}{\mathrm{PT}} \tag{6}$$

Fig. 7 shows the performance plot obtained using symmetric wavelet. The average values obtained for MRI and XA are shown.

It can be seen from Fig. 6 that the GOF 16 yields the best result.

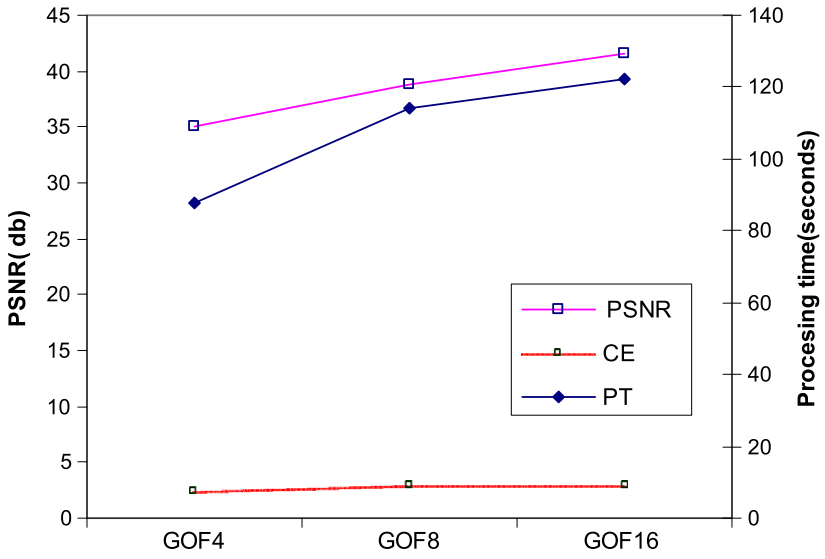

Fig. 7. Overall performance characteristics.

5. Conclusion

This paper discusses the performance evaluation of 3-D medical image using 3-D wavelet coders. Four symmetric and decoupled wavelet transforms, Daubechies 4, Daubechies 6, Cohen–Daubechies–Feauveau 9/7 and Cohen–Daubechies–Feauveau 5/3 have been used in the first stage with encoders such as 3-D SPIHT, 3-D SPECK and 3-D BISK used in the second stage for the compression. Two medical images, magnetic resonance images (MRI) and X-ray angiograms (XA) with group of slices (GOS) 4, 8 and 16 respectively were considered. The performance of the two-stage schemes has been evaluated using the bit rate and PSNR. It has been found from the experimental results that the symmetrical wavelet performs better than decoupled wavelet transform. It can be concluded that the Cohen–Daubechies–Feauveau 9/7 (CDF 9/7) wavelet in the first stage with 3-D SPIHT encoder in the second stage has been identified as the optimal wavelet–encoder for the compression of 3-D medical images. The GOS consisting of 16 slices was found to be the optimum GOS.

References

[1] P. Schelkens, A. Munteanu, J. Barbarien, M. Galca, X. Giro-Nieto, J. Cornelis, Wavelet coding of volumetric medical datasets, IEEE Trans. Med. Imaging 22 (2003) 441–458.
[2] R. Srikanth, A.G. Ramakrishnan, Contextual encoding in uniform and adaptive meshbased lossless compression of MR images, IEEE Trans. Med. Imaging 24 (2005) 1199–1206.
[3] X. Wu, T. Qiu, Wavelet coding of volumetric medical images for high throughput and operability, IEEE Trans. Med. Imaging 24 (2005) 719–727.
[4] S.C. Tai, Y.G. Wu, C.W. Lin, An adaptive 3-D discrete cosine transform coder for medical image compression, IEEE Trans. Inform. Tech. Biomed. 4 (2000) 259–263.
[5] R. Shyam Sunder, C. Eswaran, N. Sriraam, Performance evaluation of 3-D transforms for medical image compression, in: IEEE International Conference on Electro Information Technology, 22–25 May 2005, p. 6.
[6] Z. Xiong, X. Wu, S. Cheng, J. Hua, Lossy-to-lossless compression of medical volumetric data using three-dimensional integer wavelet transforms, IEEE Trans. Med. Imaging 22 (2003) 459–470.
[7] W. Badawy, W.M. Weeks, Z. Guoqing, M. Talley, M.A. Bayoumi, MRI data compression using a 3-D discrete wavelet transform, IEEE Eng. Med. Biol. Mag. 21 (2002) 95–103.
[8] P.K. Meher, T. Srikanthan, J. Gupta, H.K. Agarwal, Near lossless image compression using lossless Hartley like transform, in: Proceedings of IEEE Joint Conference on Informations, Communications and Signal Processing, vol. 1, December 2003, pp. 213–217.
[9] G. Barlas, S. Kostomanolakis, S.C. Orphanoudakis, DICOM image compression using a hierarchy of predictors, in: Proceedings of the 23rd Annual International Conference of IEEE Engineering in Medicine and Biology Society, vol. 3, October 2001, pp. 2445–2448.
[10] N.R. Wanigasekara, Shenghao Ding, Yan Zhuangzhi, Yongqin Zeng, Quality evaluation for JPEG 2000 based medical image compression, in: Proceedings of the 24th Annual International Conference of IEEE Engineering in Medicine and Biology Society, vol. 2, October 2002, pp. 1019–1020.
[11] H. Chao, J. Dong, Y.F. Zheng, G. Zhigang, Optimal 3D coefficient tree structure for 3D wavelet video coding, IEEE Trans. Circuits Syst. Video Technol. 13 (2003) 961–972.
[12] D. Gibson, M. Spann, S.I. Woolley, A wavelet-based region of interest encoder for the compression of angiogram video sequences, IEEE Trans. Inform. Tech. Biomed. 8 (2004) 103–113.
[13] X. Tang, W.A. Pearlman, J.W. Modestino, Hyperspectral image compression using three-dimensional wavelet coding, Proc. SPIE 5022 (2003) 1037–1047.
[14] J.E. Fowler, J.T. Rucker, 3D wavelet-based compression of hyperspectral imagery, in: C.I. Chang (Ed.), Hyperspectral Data Exploitation: Theory and Applications, John Wiley & Sons, Inc., NJ, 2007.
[15] Z. Lu, W.A. Pearlman, Wavelet video coding of video object by object-based SPECK algorithm, in: International Symposium on Picture Coding Symposium (PCS-2001), 25–27 April 2001, pp. 413–416.
[16] J.T. Rucker, J.E. Fowler, Coding of ocean-temperature volumes using binary set splitting with k-d trees, in: Proceedings of the International Geoscience and Remote Sensing Symposium, Anchorage, September 2004, pp. 289–292.

[17] W. Sweldens, The lifting scheme: A construction of second generation wavelets, SIAM J. Math. Anal. 29 (1998) 511.
[18] A.T. Deever, S.S. Hemami, Lossless image compression with projection-based and adaptive reversible integer wavelet transforms, IEEE Trans. Image Process. 12 (2003) 489–499.
[19] C.S. Burrus, R.A. Gopinath, H. Guo, Introduction to Wavelets and Wavelet Transforms, Prentice–Hall International, 1997.
[20] J.E. Fowler, QccPack: An open-source software library for quantization, compression, and coding, in: A.G. Tescher (Ed.), Applications of Digital Image Processing XXIII, San Diego, CA, in: Proc. SPIE, vol. 4115, 2000, pp. 294–301.
[21] V. Bhaskaran, K. Konstantinides, Image and Video Compression Standards Algorithms and Architectures, Kluwer Academic Publishers, 1996.
[22] C. He, J. Dong, Y.F. Zheng, Z. Gao, Optimal 3-D coefficient tree structure for 3-D wavelet video coding, IEEE Trans. Circuits Syst. Video Technol. 13 (10) (2003) 961–972.
[23] J.K. Udupa, G.T. Herman, 3D Imaging in Medicine, CRC Press, 2000.
[24] Z. Wang, A.C. Bovik, H.R. Sheikh, E.P. Simoncelli, Image quality assessment: from error visibility to structural similarity, IEEE Trans. Image Process. 13 (2002) 600–612.
[25] B. Ramakrishnan, N. Sriraam, Internet transmission of DICOM images with effective low bandwidth utilization, J. Digital Signal Process. 16 (6) (2006) 825–831.
[26] R. Shyam Sunder, C. Eswaran, N. Sriraam, Medical image compression using 3-D Hartley transform, Comput. Biol. Med. 36 (9) (2006) 958–973.

N. Sriraam received his B.E. (ECE) from National Engineering College, India and M.Tech. (Biomedical Eng.) [Distinction] from MIT, Manipal, India. He secured the University First Rank and was awarded the gold medal in M.Tech. He was working at the Faculty of Information Technology at Multimedia University, Malaysia where he also did his Ph.D. in the area of biosignal processing. Mr. N. Sriraam is currently working as Professor and Head in the Department of Biomedical Engineering at SSN College of Engineering, Chennai, India. He has supervised four MS students in the area of biomedical signal processing and bioinformatics. He has published 30 articles in international journals and has been involved in several sponsored research projects. His research area includes biomedical signal and image processing, data mining, neural networks. He is a senior Member of IEEE and member of IEEE EMBS.

R. Shyamsunder received his BE degree from University of Madras, India in 2003 and Masters in Information Technology from Multimedia University, Malaysia. His research interests are 3-biomedical and video signal compression using wavelets and other techniques. Currently he is doing his PhD at the Electrical and Computer Engineering Department at the National University of Singapore. He is a student member of the IEEE.